We are IntechOpen,
the world's leading publisher of
Open Access books
Built by scientists, for scientists

4,800
Open access books available

122,000
International authors and editors

135M
Downloads

154
Countries delivered to

Our authors are among the

TOP 1%
most cited scientists

12.2%
Contributors from top 500 universities

BOOK CITATION INDEX INDEXED

WEB OF SCIENCE™

Selection of our books indexed in the Book Citation Index
in Web of Science™ Core Collection (BKCI)

Interested in publishing with us?
Contact book.department@intechopen.com

Numbers displayed above are based on latest data collected.
For more information visit www.intechopen.com

Magnetic Pulse Welding: An Innovative Joining Technology for Similar and Dissimilar Metal Pairs

T. Sapanathan, R. N. Raoelison, N. Buiron and
M. Rachik

Additional information is available at the end of the chapter

Abstract

Once it was widely thought to be an exceptional innovative welding solution, the magnetic pulse welding, dragged the related manufacturing industries and particularly automobile companies for its complex assembly solutions in early 2000s. Although this technique has been implemented by some giant manufacturers for various joining tasks, the process still has not been well adopted by industries. However, in recent years, many researchers turned their attention to the potential applications and insight investigations of this process due to the existence of bottlenecks and the prime novelty of this technique. This chapter clearly highlights the process, applications, requirements, interfacial kinematics of the welding, numerical predictions of interfacial behaviours and multi-physics simulations. This chapter recommends that the overall outlook of the process is promising while it requires extra attention in the individual welding cases and its material combinations.

Keywords: magnetic pulse welding, interface, numerical modelling, weldability, plastic deformation

1. Introduction

Recently, multi metallic hybrid materials have been produced by joining dissimilar metals at their solid state [1–5]. Those types of materials become attractive in modern engineering applications as they can provide multiple attributes in a single solution [6–9]. The magnetic pulse welding (MPW) is an innovative joining technology that has been mainly considered for this purpose [10]. This technology involves a significantly high speed collision and high strain

rate plastic deformation. In general, the workpiece experiences a strain rate of up to 10^2–10^4 s^{-1} [11] while this could reach an ultimate value of 10^6–10^7 s^{-1} at an interface [12]. The synergetic effect between electromagnetic phenomena with metal plasticity contributes towards the advantages of this process in comparison with conventional and other high speed welding techniques. However, this process has not been widely implemented until now, even though it is known since late 1960s [13, 14] and its booming advantages have been paid attention by automotive manufacturers in early 2000s. That is, large scale implementation of this technology has always been challenged by the existence of unique complex realities of this process. But, fortunately, recent technological advancements allow for thorough investigations to understand the physical phenomena of this multi-physics process and facilitate an effective utilization of the technology into modern engineering applications. Emerging scientific technology provides more room to explore such high speed manufacturing processes using sophisticated engineering tools such as high speed measurements, experimental observations, microscopic analyses and advance computing techniques.

MPW is believed to bring innovative solutions in joining technology and the merits of the process are covered in this context. The objectives of this chapter are divided into five main sections including position of the MPW today and its potentials, description of the process, weld features and variance, identification of the weld nature by simulating the interface behaviour during the collision, and computation of the in-flight dynamics using coupled multi-physics numerical simulations.

2. Position of the MPW process today and its influences

Joining processes technically and financially offer strong potentials and represent a significant global market. An overview of the added value brought by the joining activities is briefly presented to address the growing interest in this engineering field. This part of the chapter explains the technical-economic status of the welding technology including recent developments in 2005–2007 about the added value with its increasing trend for the global market of the welding. Current status of the technical evolution marks a major technological transition with the emergence of the solid state welding method for the MPW. A brief review of the technical solutions developed by MPW is addressed. It also provides various representations of successful configurations, suitable combinations of materials and major advantages offered by the MPW process.

2.1. Socio-economic influences of the joining and welding processes

A recent survey focused on the European zone provides data related to the technical and financial consequences of the joining technology and the added value brought by the joining manufacturing activities [15]. In the case of Germany, the data gives a representative indication since this country is the leading manufacturer of joining machines which represent about one-third of the EU's production [15]. Available data inform that, for this country alone, the added value generated by the assembly industry is increased more than 22 billion euros by 2000s

without any significant decrease [15], which corresponds to a proportion of 26% increase at European level. But contributions of other countries are also important; this includes Italy, France, Poland and United Kingdom which have respectively provided 18%, 10%, 9%, and 8% [15]. This assessment does not include either the worldwide data or the recent data, but represents an indication of the socio-economic influence of the joining technology.

Welding activities generally cover a substantial part of the assembly industry. For reference purposes, they returned a total market turnover of 19.3 billion euros for Germany in 2003, providing 6% of the jobs linked to this industry, which represents 1.7% of increase in employ‐ment opportunities including all sectors [16]. A comparative study carried out between 2001 and 2005 has shown an added value increased by 18% of job creation including 5% directly linked to the welding activities [16]. Such expansion highlights the socio-economic benefits brought by the welding technology. Furthermore, note that the welding represents a non-negligible investment in several industrial branches including the most advanced sectors in transportations, energy and medicine.

In the specific case of metal joining, welding methods bring some useful flexibilities. It does not require intermediate joining component (bolt, rivet, adhesive layer, brazing material etc.) allowing thereby possibilities to produce structures with the benefits of cost and weight reduction. A weld can confer as a permanent joint which is suitable for many mechanical performances. In addition, the welding methods can be applied at varied length scales, from micrometric (micro welding) to several hundreds of millimetres. Furthermore, welding practices include several techniques and processes, making them robust, widely used and intrinsic to technological advances and innovations.

2.2. Innovative nature of the electromagnetic pulse technology (EMPT)

Conventional welding processes show difficulties in joining new metal combinations. The current innovations increasingly introduce dissimilar assemblies that enable to meet new challenges such as light weight requirement, structural reinforcement, and other functional specifications. In this respect, innovative solutions have led to the consideration of complex functional material combinations including metallic assemblies with different melting temperatures, where the fusion welding processes fail when producing such joints at the interface. The discrepancy between the melting points of two dissimilar metals prevents a successful joint formation by solidification of a molten pool as usually achieved during a fusion welding process. The exploration of new methods have led to various welding principles among which high velocity impact welding (HVIW) methods enable bonding dissimilar metallic combinations. High pressure, short duration and low temperature bonding form the main particular characteristic of these methods [17]. The welding involves a strong interfacial collision in various high velocity impact methods using the explosive detonation (explosive welding), the laser shock impulse (laser spot welding), the magnetic impulse (MPW), or the vaporizing foil actuation (vaporizing foil actuation welding).

The use of electromagnetic impulse to provide a significant Lorentz force makes the MPW as an attractive method with respect to other high speed collision welding processes. The EMPT is particularly different in terms of cost, reliability, ease of use, flexibility, rate of work, no

Figure 1. EMPT for industrial applications implemented by "PSTproducts" (a) Al/Cu electric bus bar [www.pstproducts.com], (b) EMPT crimped gear box part [www.pstproducts.com] (c) EMPT welded Al pressure vessel for air conditioning system [28], (d) EMPT welded Al/steel crash box [www.pstproducts.com], (e) EMPT welded Al/Cu cooling plate [www.pstproducts.com] (f) EMPT crimped Al/steel tube instrumental panel beam [28], (g) EMPT for hemming of a Al pressure vessel [28], (h) EMPT crimped Al lid on a pharmaceutical glass bottle [29], (i) EMPT crimped drive shaft [28] and (j) EMPT crimped air suspension [28].

requirement of being consumable and eco-efficiency [18]. This method simply uses a standard electrical source intermittently and a magnetic coil. The welding test does not require either a surface treatment or a long experimental preparation, and is performed in a very short period of time, i.e. it only takes less than a few hundred microseconds to produce a joint. This is a precise joining method that has been successfully applied on several similar and dissimilar metallic combinations for different configurations such as overlap, half lap, cross lap, end lap etc. This joining method is also suitable for various geometrical components including tubular assembly, plates or any specific shape. It is possible to generate a complex distribution of a magnetic pulse force due to the strong flexibility of electromagnetic welding tool design [19]. Current potentialities of the EMPT are depicted by Kapil et al. [18]. The authors addressed a comprehensive review of successful applications, where some are being industrialized, and the growing interest given to the process in several industrial sectors such as in automobile, aerospace, nuclear, electrical and microelectromechanical systems (MEMS), ordinance and packaging [18]. Although the pragmatic results are numerous, concisely its applications are well suited to any tubular assembly, regular or irregular shapes, as well as to any flat shape connections (**Figure 1**). EMPT is successfully implemented to perform various manufacturing tasks using semi and fully automated lines by "PSTproducts GmbH" that also offers engineering and industrial solutions including a robotic arms to effectively handle the portability of the unit in industrial welding cases (**Figure 2**) [20]. In addition, the process covers a broad range of material combinations including Cu/Zr-based metallic glass [21], Al/metallic glass [22], Cu/Manganin [23], flexible circuit boards [24], Cu/Brass, Cu/steel, Cu/Al, Al/steel, Al/Mg, Al/Ni, Al/Fe, Al/Ti and Ti/Ni [25–27]. With all these aforementioned benefits, the EMPT is continuously explored and progressively optimized to bring new potential advancements for effective industrial implementation.
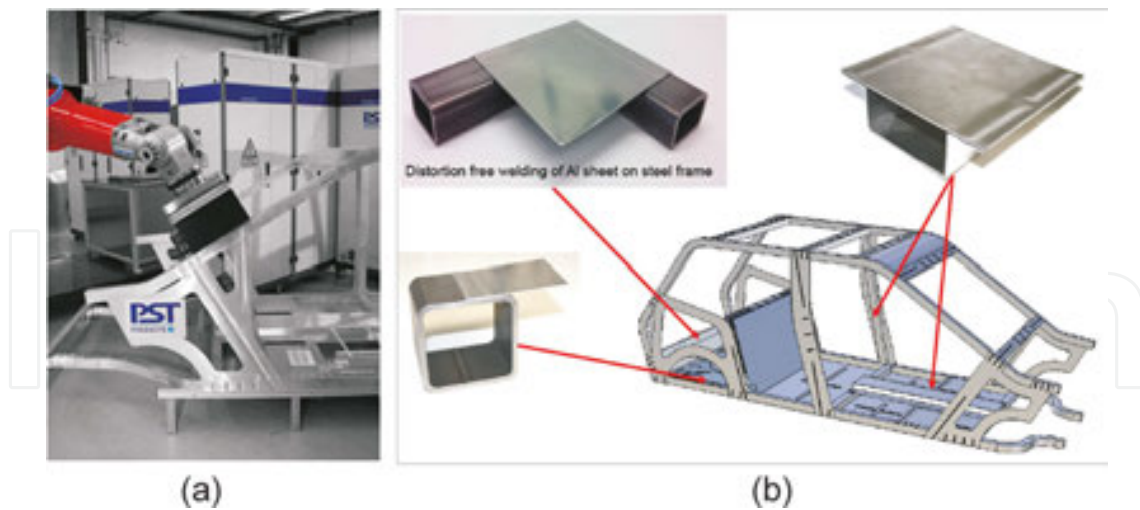
Figure 2. (a) Automated robotic arm used to implement EMPT during a Body in White (BIW) construction and (b) various welded components produced using the robotic arm by "PSTproducts" [20].

3. Description of the MPW process

In general, the MPW process is a user-friendly joining method. The working principle of the process is simple and the welding procedure is fast, easy, and viable. This section briefly explains the general principle of the process including the architecture of the welding machine and the welding parameters. Interactions between process and welding parameters are provided including the specifications of their controllable and measurable natures. This gives a holistic understanding of the process principle with different variables involved in the selection of the welding parameters.

3.1. Magnetic pulse welding architecture

Figure 3 shows typical magnetic pulse welding architecture with overlap configuration used to weld a core clad combination. The MPW is sufficiently flexible to weld various shapes of components for different joint configurations such as half lap, overlap, cross lap and end lap (Section 2.2). Basically, a MPW setup consists of a pulse generator, a coil and an optional field shaper. The generator contains a transformer which transforms a low-voltage power supply into a high voltage charge in the range of kilo-Volts stored in a capacitor bank. This generator set, connected to an inductive coil through a control switch, delivers a high discharge current in the range of a few hundred kilo-Ampere. The electric discharge flowing through the coil generates a magnetic field which creates significantly large Lorentz force within the external tube (the flyer) in the case of a tubular assembly. Thus, the flyer tube undergoes a high strain rate plastic deformation and collides onto the fixed inner rod to produce a high velocity collision. The discharge pulse frequency depends on the parameters of the electromagnetic circuit (Equation 1) and which lies in between 10–200 kHz, but usual operational frequencies are in between 10–20 kHz during the applications. The inductive multi turn coil can be used

with a field shaper that concentrates the magnetic field in the working area while increasing the magnetic field intensity. Moreover, one can also control the electromagnetic field and consequent deformation of the material by utilizing various geometries of the field shaper for the same coil [30]. The process can also be performed without the field shaper depending on the required process parameters, or the coil itself can be manufactured which includes the field shaper geometry, especially suitable for single turn coils. However, using a multi turn coil with a single turn field shaper is the notable practice in the current manufacturing that reduces the replacement cost in case of damage of either tool. **Figure 3** shows a MPW configuration including a coil with a separate field shaper and also indicates the direction of the electromagnetic forces on the external tube where the compressive Lorentz force facilitates the deformation of the flyer tube.
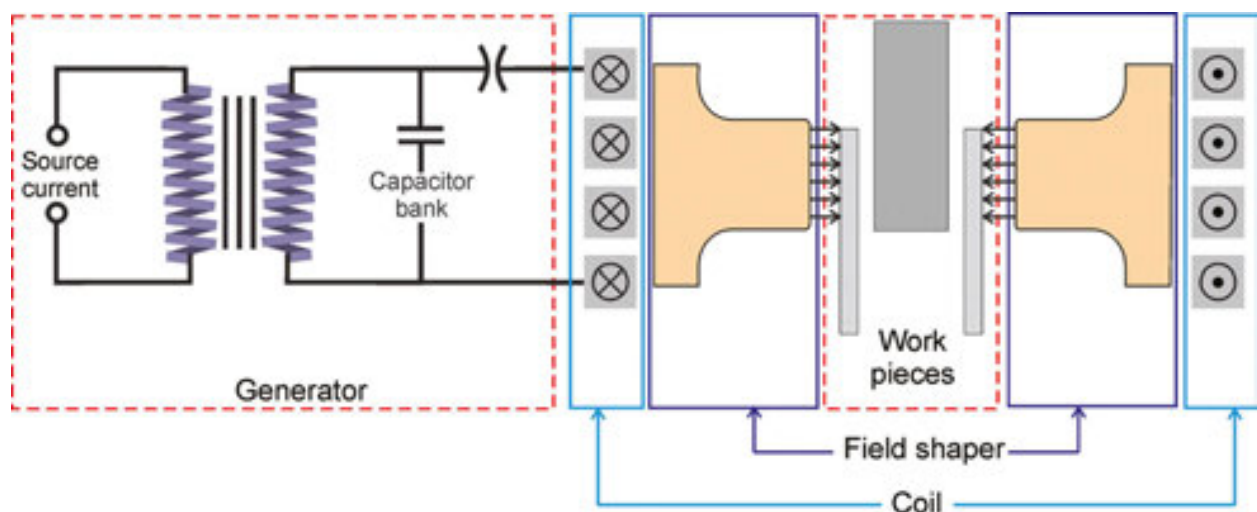

Figure 3. A typical architecture of the MPW and crimping of tubular assemblies used in overlap configuration.

The circuit frequency *f* can be determined by other parameters using Equation (1).

$$f = \frac{1}{2\pi}\sqrt{\frac{1}{LC}}$$

(1)

Where *L* is the circuit total inductance (H) and *C* the capacitance of the generator (F).

3.2. Description of the influencing parameters and working conditions

Basically, a MPW test consists of a simple procedure. The workpieces are placed inside the working section for a tubular assembly. Diameters of both flyer and inner rod determine the air gap, which lies in between the inner surface of the flyer and the outer surface of the rod. The formation of the joint in the overlap configuration decides the weld length depending on

the inserted lengths of both the rod and tube inside the working area in an assembly. The MPW user prepares this installation where the initial air gap is one of the main geometrical parameter affecting the collision condition, and thus the weld formation. A command console allows for setting up the discharge voltage that is the main adjustable parameter controlling the welding test. The discharge voltage value is indicated as it is or in terms of discharge energy (E) given by Equation (2).

$$E = \frac{1}{2} CU^2 \tag{2}$$

Where E is the discharge energy (J), C the used total capacity of the bank capacitor (F) and U the discharge voltage (V). Generally, the discharge voltage and the initial air gap provide a set of controllable parameters denoted as (U, g). They are indicated for each corresponding welding test. However, the discharge pulse frequency also becomes a crucial process parameter since it decides the penetration of the magnetic field from the coil through the thickness of the flyer. This creates an eddy current in the external region of the flyer that penetrates in accordance with the skin depth defined by Eq. (3). The interaction of the eddy current with the magnetic field from the coil produces the Lorentz force that accelerates the flyer till its onset of collision with the inner rod. Hence, without the skin depth effect, the motion of the flyer is impossible. Therefore, for an effective collision, the discharge pulse frequency should be selected to generate a skin depth lower than the wall thickness of flyer. Eq. (3) also provides an indication of the influence of skin depth on the discharge pulse frequency. More details of the skin depth could be found elsewhere [31].

$$\delta = \sqrt{\frac{\rho}{\pi f \mu_o}} \tag{3}$$

Where δ, ρ, f and μ_o respectively denote the thickness of the zone affected by the skin depth effect (m), the electrical resistivity of the flyer (Ωm), discharge current frequency (Hz) and magnetic permeability in free space.

High frequency current is generally recommended for high resistive metals. One should also carefully consider the discharge pulse frequency of a setup requirement for a generator that also modifies the capacity of a welding machine. In addition, increase in discharge frequency reduces the impulse duration that subsequently increases the strain rate of the flyer and the consequent dynamic response of the material and collision conditions. Those interrelated effects can make difficult in the selection of a suitable discharge frequency that is conducive to provide expected results. Generally, the discharge voltage and the air gap are the most adjustable parameters for a MPW test. The discharge pulse frequency value is indicated by an experimental measurement using a Rogowski probe.

4. Interface behaviour and weld variances

In a conventional welding process, a weld is basically defined by three distinct zones: the solidified molten zone at the joint, the surrounding heat affected zone, and the base metals whose properties remain the same. The weld is generally produced at large scale to ensure an efficient joint at the interface during a conventional welding process. But, in MPW, since the bonding principle is completely different, the notion of weld nature is particularly varied in term of size and morphology. High velocity impact welds are typically confined at the interface within a few micrometre thick zones. A permanent bond occurs immediately between the two components but the behaviour of the interface represents different weld variances. Investigations of welded specimens from Al6060-T6/Al6060-T6 joints have allowed identifying the typical variances for a similar metal pair [32–35]. The major observations of such investigations are reported in the following sections, which also cover the effect of joining dissimilar combinations.

4.1. Onset of weld without apparent interfacial deformation

The interface experiences a progressive kinematic phenomenon that governs the generation of various interfacial morphologies when subjected to the high speed collision. In MPW, the weld natures are generally identifiable at the microscopic level, and the first case is an apparent bonding showing a metal continuity across a straight bonded interface (**Figure 4**). This corresponds to the onset of weld produced by a predominant high compressive stress which is a hydrostatic stress since the grains adjacent to the interface remain undeformed (**Figure 4**). The interfacial zone exhibits an equiaxed grain structure without any noticeable deformation supporting the bond formation due to hydrostatic stresses. Generally, the contact pressure is expected to be in the range of 1–20 GPa according to a simple assessment based on the expression of collision pressure $P = \rho_1\rho_2 C_1 C_2 V_i / (\rho_1 C_1 + \rho_2 C_2)$, where ρ_1 and ρ_2 are the material densities, C_1 and C_2 are the speed of longitudinal waves in those materials and V_i is the impact velocity. The welded joint can extensively be straight as long as the interface remains stable during the complete collision (**Figure 4b**). The hydrostatic bonding is uniform along the interface and the collision is essentially governed by a normal stress. However, due to the oblique collision, the tangential component of the impact velocity can be high enough to cause
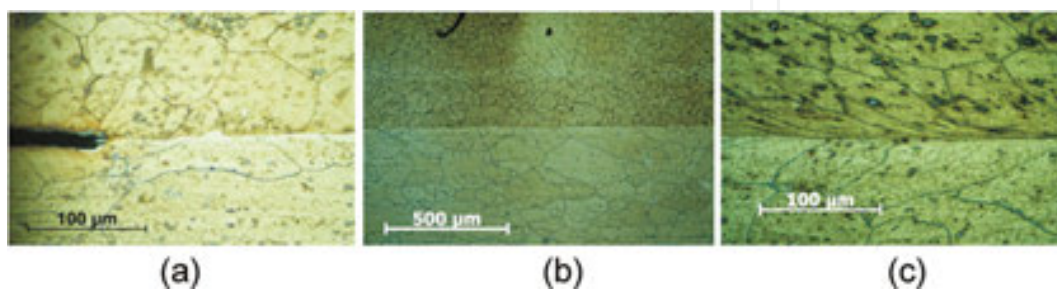

Figure 4. Typical interfacial features of an onset of bonding [32, 33]: (a) magnified view of a straight bonded interface, (b) typical large bonded zone and (c) typical bonded interface with onset of interfacial shearing.

a shearing action at the interface. Therefore, as a result of the confined shearing, the nearby grains at the vicinity of the interface become flattened and elongated as shown in **Figure 4c**.

4.2. Interfacial deformation and wavy nature of the bonded interfaces

The interfacial shearing causes a series of kinematic instabilities that changes the morphology of the interface whose behaviour is therefore similar to the Kelvin-Helmholtz instability that occurs at fluidic interfaces subjected to an interfacial shearing. The straight interface becomes wavy at the onset of instability. The development of wave at the interface is governed by two main phenomena: interferences of compressive shock waves due to the dynamic collision and a jetting phenomenon governed by an alternate inversion. As suggested by Ben-Artzy et al., the first phenomenon is a mechanism for the creation of periodic humps with regular shapes [36]. The wave height and periodicity depend on the size of the structure, the compressive stress intensity, and the interference of shock waves along the interface. Under these conditions, the initiation and development of hump can be considered as a consequence of deformation of the bonded and sheared interface by the reflection of mechanical waves. All the humps regardless of their amplitude reveal shear strain along the interface that would be regularly shaped the wavy interface (**Figure 5**).
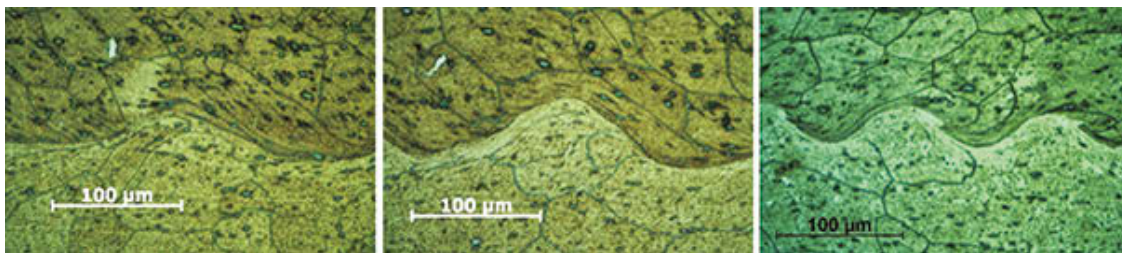

Figure 5. Typical magnetic pulse welded interfaces with wavy morphologies showing grains shearing along the wavy pattern [32, 33].

4.3. Jetting phenomenon and interfaces with irregular wavy shapes

The interfacial shearing can reach an instability threshold due to a high strain rate and severe shearing. In the literature of impact welding, a notion of shear instability is used to demonstrate this circumstance. The confined shearing remains at the interface, but becomes abruptly excessive so that a jetting phenomenon occurs. A tangential jet forms ahead of the collision point and the jet kinematics is controlled by the normal force component along the interface that develops from both shock waves and impact velocity. The jet may evolve following a series of upward and downward jetting to form a sequence of inverted curves along the interface. In that way, the interface develops by jetting phenomenon which is interpreted as both a weld indicator and a mechanism of interfacial humps formation. However, the kinematics of the sheared interface is complex so that it is difficult to clearly state which mechanism really forms the wavy interface: the interference of compressive shock waves or the jetting phenomenon. These two factors can be concomitant or asynchronous or due to their consequences. Particularly, for regular shape humps, a simultaneous prominence may prevail as

observed in **Figure 6**. The deformation of the interface creates a hump with nearly symmetric shape (regular shape) while the grains adjacent to the bonded interface are strongly sheared with an upward kinematics at the left front of the hump and a downward kinematics at the right front (**Figure 6a**). If the jetting phenomenon becomes predominant, irregular shapes arise from the progression of humps. A jetting aspect and its orientation can be clearly observed that depend on the governing stresses. On the typical case evidenced in **Figure 6b**, a downward jet occurs. This could initially be an upward jet that is inverted by an interference of shock waves at the interface, or a pure downward jet guided by the local stress evolution, or kinematic instability governed by an opposed shear alone similar to that of Kelvin-Helmholtz instability occurs at fluidic interfaces subjected to a shearing. Hence, the mechanism of wavy interface formation is to be fully explored despite the experimental identification of particular morphologies.
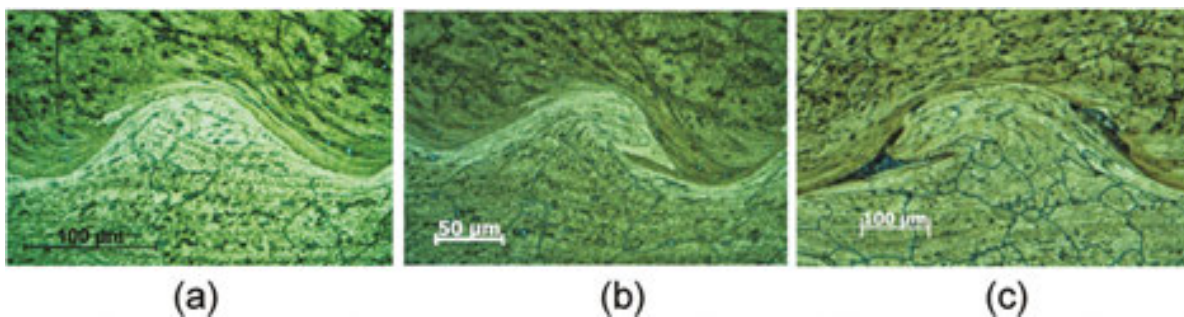

Figure 6. Wavy morphology with strong confined shearing, jetting, irregularly shaped interface and defect onset [32, 33]. (a) Wave formation with upward kinematics, (b) downward kinematics and (c) wavy interface with onset of defects.

4.4. Vortex development and formation of defective welds

Generally, the wavy shape is identified as a particular feature of a high speed welded joint and it has also been suggested as a weld indicator. Nevertheless, distinction between regular and irregular development of wavy interfaces could be useful. Formations of irregular humps due to the predominance of the jetting phenomenon indicate a severe shearing that can promote a confined heating. The plastic work can also be high enough to cause a strong thermomechanical softening, even a melting, and thus the strong shear stress would be unfavourable in the weld formation. Potential matters from ejection also lead to the formation of cavities within the welded interface. The interfacial observation in **Figure 7** represents a typical onset of defects appearing within the irregular wavy interface produced by the jetting phenomenon. Formation of holes is evidenced at the jet tip and at the vicinity of the strongly sheared interfaces (**Figure 7**). Moreover the defects are confined at the bonded joint. The defective weld can be also caused by the kinematic progression of the interface. The jet flow may evolve towards complex kinematics such as a swirling flow. Zones of jetting occurrence become potential sites of vortex development similar to the Kelvin-Helmholtz instability in fluids. Experimentally, it was evident that the jetting affected zone (JAZ) containing prominent voids with circular morphology supports the suggestion of vortex development (**Figure 7**). These voids increase

in size at the vortex affected zone (VAZ), and their enlargement depends on the local kinematics and stress distribution. Note that the size of voids can reach up to several hundred μm, in the same range of the height of the humps, i.e. approximately equal to the size of the weld width. The mechanism of void formation could be due to an ejection molten fluid, a solidification shrinkage or a local fragmentation combined with particulates jetting governed by shear stresses [32]. In any event, the welded interface becomes defective due to the formation of discontinuous voids (**Figure 7**).
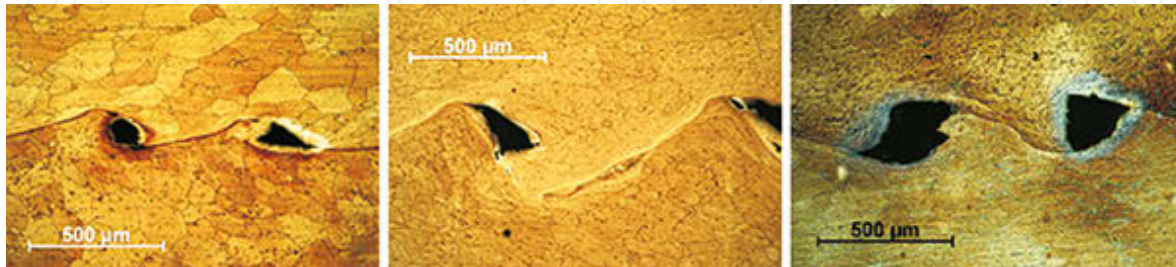

Figure 7. Typical magnetic pulse welds with defects at the VAZ [33, 34].

The MPW of similar metal pairs generally reveal the weld natures among those aforementioned variances. This large depiction is useful to identify the weldability. It is clear that the single case of wavy morphology is not sufficient to substantiate the weld formation as commonly suggested. Although this weld indicator is valuable, the bonding is able to occur independently of the interface shape thus the development of humps can evolve a defective joint. In addition, the relevance of wavy morphology is discussed for dissimilar metal combinations. However, this situation is identified as no longer a reliable consideration of a bond formation. Albeit the literature of impact welding includes several cases of regular or irregular wavy shaped dissimilar joints, there exist some cases where the formation of humps is conducive to brittle joints. This scenario was found when replacing the previous Al6060-T6/Al6060-T6 pair by a dissimilar Al6060-T6/Cu combination, the copper being the inner rod in order to ensure the same in-flight behaviour for the flyer prior to the collision. Further investigations for in-flight behaviour of similar and dissimilar cases are also explored using multi-physics simulations in Section 6.

4.5. Weld with an interfacial mixing or intermetallic compounds

In term of material dissimilarity, the copper is softer, having a higher melting temperature and dissipating the interfacial heating more quickly than those of the aluminium alloy. The combination of these properties produces a different response at the Al/Cu interface during the collision. In contrast to the previous case (Al/Al), the major noticeable changes are associated with the interface nature and particularly prominent with the vortex development. When the vortex instability develops, the copper forms a solid spiral due to its higher malleability and higher melting temperature than those of the flyer part. The VAZ consists of a roll-up so that the copper and the aluminium are locally intermixed (**Figure 8a**). The kinematics of the vortex contributes to the interface bonding by an interlocking mechanism governed by the

intermixing phenomena. Note that the vortex instability evolves at high strain rate and excessive deformation so that the plastic work heating enables to melt the aluminium during the swirling phenomenon. The molten phase is quickly solidified due to confinement of the heating and the rapid heat dissipation is facilitated by the good thermal conductivity of both copper and aluminium. These two factors promote a high cooling rate in the range of 10^{4-6} K/s that prevents the atomic structural changes such as crystallisation during slow thermal kinetic. The hyperquenching freezes the random allocation of atoms within the initial molten phase and produces an intermetallic phase which was proven to be amorphous [37]. Hence, the dissimilar Al/Cu combination is conducive to intermetallic formation, within the VAZ and along the interface that alters the physical nature of the weld. The intermetallic phases may appear within discontinuous pockets (**Figure 8b**) or as a continuous layer with a non-uniform thickness (**Figure 8c**). In any case, the presence of the intermediate intermetallic media introduces a new weld variance that is particularly suggested for dissimilar metal joints produced in MPW.
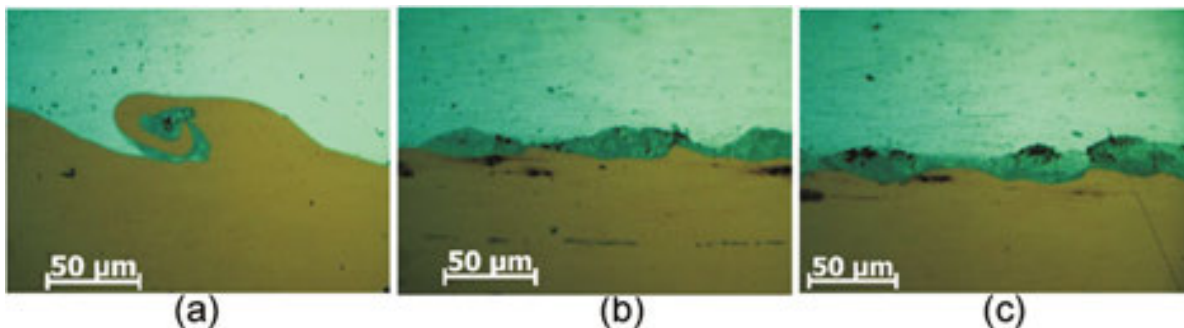

Figure 8. Typical dissimilar magnetic pulse welds with (a) vortex development, (b) intermetallic pockets and (c) continuous intermetallic layer at the interface [33].

4.6. Fracture within intermetallic phases and detrimental welds

The formation of a permanent bonding becomes difficult with the accumulation of intermediate intermetallic compounds (IMCs). The fast shrinkage during the solidification stage involves cold cracking phenomenon governed by the heterogeneous heat conduction combined with the incompatibilities of the thermal expansion coefficient. For the case of thin IMC layer, light microscope observations at low magnification reveal transverse cracks across the thickness without further propagations outside the intermetallic zone (**Figure 9a**). These microcracks randomly coalesce and formarbitrary multidirectional crack propagation. The intermetallic media facilitates the cracks to fragment which lead to a catastrophic failure of the joint (**Figure 9b**). It was evidenced that the thickening of the intermetallic phase is favourable to form numerous cracks so that its occurrence can strongly impair the weld integrity. Eventually, the interface can completely break due to a propagation of a macro crack within the intermetallic zone along the interface. According to experimental analyses, this major fracture is attributable to the development of predominant shrinkage stresses during the intermetallic solidification or to a detrimental shearing stress arises from the liquid or solid

ejection of intermetallic phases from the interface [33–35]. Finally, the interface debonding could be also resulted from a separation of molten IMCs from the aluminium solid wall while opening stresses could act during the confined melting. Such hypothesis was supported by experimental observations revealing typical features of a liquid that freely spreads prior to the solidification [33–35]. Indeed, the top surface of an identified intermetallic region exhibits a smooth appearance without fracture pattern due to debonding, and the heterogeneous nature of this surface evidences a free fluid flow [33]. These entire phenomena associated with intermetallic formation adversely affect the welding efficiency of dissimilar metal combinations. The sole alternative is to minimize the thickness of inter metallic layer using an identified lowest critical impact energy. Hence, from similar to dissimilar metal combination, the notion of bonding and weldability is phenomenologically different so that their identification should be accurately established. The next section is numerical simulation to reproduce the interfacial morphologies, which could be used to identify the potential weld variances including the weldability window for similar and dissimilar assemblies.
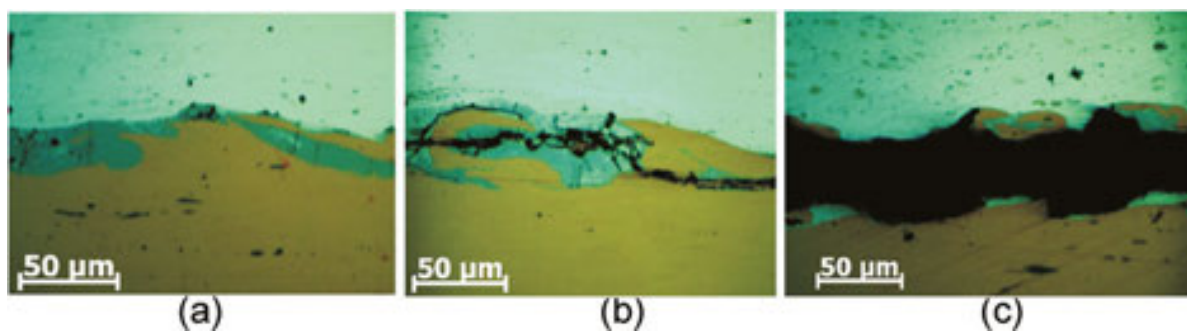

Figure 9. Typical defective dissimilar magnetic pulse welds with (a) onset of cracks within the intermetallic phases, (b) fragmentation, and (c) catastrophic failure [33].

5. Numerical simulation of the interface behaviour

This section begins with a literature survey regarding the numerical simulation of the interface behaviour during impact welding, prior to the suggestion of a suitable method, namely Eulerian simulation to compute the collision and weld generation. This method is applied for both similar and dissimilar metal combinations (Al/Al and Al/Cu) to show the convincing predictions of typical interfacial features including the wavy morphology and formation of defects.

5.1. A brief literature review of impact welding simulations

The numerical simulations of the weld generation during impact welding processes can be classified into five distinct methods known as Lagrangian, Adaptive Lagrangian-Eulerian (ALE), Eulerian, smooth particle hydrodynamic (SPH) and molecular dynamics (MD). Generally, Lagrangian computation fails during the development of excessive interfacial

shearing. Due to the large strain produced by the kinematic instability of the interface, the mesh experiences strong flattening and distortion that eventually aborted the computation [38–48]. A wavy interface is difficult to perform even the onset of jet kinematics can be detected using this method. Alternatively, ALE method is suggested to improve the mesh quality by utilizing a node relocation algorithm during the computation [39–41, 46, 49], but its real capability to produce persuasive wavy patterns has to be demonstrated. ALE method also suffers from the bad mesh quality due to the interfacial shearing and jetting. To overcome mesh issues, particle based methods were investigated among which the MD computations allow for the accurate simulation of complex interfacial morphologies but they meet a scale limitation [50–52]. MD method is rather appropriate for small scale, in the range of 10–100 nm unlike the SPH method that enables the computation of the interfacial jetting and wavy morphology at a large scale [42, 43, 53, 54]. However, the accuracy of the SPH method is discussed regarding the consideration of the dissipative terms [55]. The method becomes unsuitable if such physical phenomenon prevails.

At present, Eulerian computation offers a possibility to reproduce the kinematics of the interface during the collision. Generally, Eulerian method is used in computational fluid dynamics but can be applied to a solid to simulate a material flow, with acceptable results using a Johnson-Cook constitutive model for describing the material [44, 45, 56, 57]. In the literature, some simulations of weakly shaped interfaces were presented [42, 43, 50–53]. The method merits to be further explored to compute the full development of the wavy morphology as well as the defects' formation. Sections 5.2–5.4 include a description of the Eulerian procedure and convincing simulation results encouraging the enactment of such method in MPW.

5.2. Eulerian method

Eulerian method is mainly used in computational fluid dynamics that solves the conservation equation of mass, momentum and energy. The history of state variables is computed at any point (M) of a domain. The method uses a fixed computational grid and the time dependant variation of these variables on each grid describes the fluid flow. This is called pure Eulerian computation applied to Newtonian and non-Newtonian fluids. The major difference between fluids and solids relies on the description and treatment of mechanical behaviour. For the peculiar case of solid dynamic, the high strain rate dependency of the stress governs the mechanical behaviour and a constitutive law, the Johnson-Cook law, is generally used. For a suitable numerical treatment of this law, a split method is suggested to solve the governing equations of Eulerian method whose differential forms are expressed as follows:

$$\frac{\partial \psi}{\partial t} + \vec{u}.\overrightarrow{grad(\psi)} = -\psi \, div\left(\vec{u}\right) \tag{4}$$

$$\frac{\partial \vec{u}}{\partial t} + \vec{u}.\,\overrightarrow{grad(\vec{u})} = \frac{1}{\psi}\,\overrightarrow{div\left(\underline{\underline{\sigma}}\right)} + \frac{1}{\psi}\,\overrightarrow{F_v} \tag{5}$$

$$\frac{\partial e}{\partial t} + \vec{u}.\,\overrightarrow{grad(e)} = \underline{\underline{\sigma}} : \underline{\underline{D}} \tag{6}$$

where, $\psi, \vec{u}, \underline{\underline{\sigma}}, \overrightarrow{F_v}, \underline{\underline{D}}, e$ respectively denotes density, velocity vector, Cauchy stress, internal body force vector, strain rate tensor and specific internal energy which is assumed to be an enthalpy to compute the heating due to the plastic work $\underline{\underline{\sigma}} : \underline{\underline{D}}$.

The split strategy consists of an operation that decomposes each conservation equations into two parts in order to separately compute advection variables. In a one dimensional form, the generic conservation equation is given by (Equation 7) and the splitting gives the pair of equations (Equations 8 and 9).

$$\frac{\partial \varnothing}{\partial t} + u_x \frac{\partial \varnothing}{\partial x} = F \tag{7}$$

$$\frac{\partial \varnothing}{\partial t} = F \tag{8}$$

$$\frac{\partial \varnothing}{\partial t} + u_x \frac{\partial \varnothing}{\partial x} = 0 \tag{9}$$

Equation (8) represents the usual dynamic equation of solid which is solved by the usual Lagrangian method, i.e. the mechanical computation of spatio-temporal motion given by the mesh deformation depending on the material behaviour. This is called the Lagrangian step. Afterwards, the converged state variables given by the Lagrangian step are advected using Equation (9) on spatial fixed mesh. This is called the Eulerian step during which the advection computes the material flow. The material interface is calculated by the volume of fluid (VOF) front tracking method. The sequential Lagrangian/Eulerian computation eliminates the problems of mesh distortion and flattening, thus enables to reproduce the complex kinematics of the interface during the collision progression.

5.3. Virtual testing of the wavy interface generation

Virtual tests are performed under the same conditions as for the experimental results provided in Section 4. **Figure 10** shows the results obtained from a 2D simulation. First computation

considers a similar Al/Al combination with a flyer thickness of 1.5 mm and an air gap of 2 mm. A Johnson-Cook law is used to describe the material behaviour with the assumptions of isotropic hardening, a von Mises yield surface and a geometric non-linearity.

The Eulerian finite element computation can provide accurate predictions with respect to the weld generation and the singular feature found in impact welding including the development of interfacial wavy morphology during the collision progression. In **Figure 10**, the collision propagates from the right to the left. The bonding begins with a straight interface as previously described in the Section 4.1. Although, this situation can be computed successfully by a usual Lagrangian method based on a mesh deformation, it fails to produce the wavy interface. In contrast, Eulerian computation enables the simulation of the weak or big waves' formation along the interface as clearly shown in **Figure 10**. The complex kinematics of jetting is reproduced with a fine description of the material interface. **Figure 11** shows three types of typical jetting stages ahead of collision points. Developments of successive inverted jets [downward (**Figure 11a**) and upward (**Figure 11b**, **c**)] are evidenced. The material flow governed by this jetting phenomenon forms the progressive wavy morphology. Ejection of particles is also evidenced in the simulation. In the numerical point of view, this result arises from the advection procedure that calculates the temporal evolution of each state variable over the computational grid. Material flows occur where they are expected to appear. Note that the ejection is a physically realistic phenomenon in MPW. It was evidenced that solid fragments or aggregates are ejected from the interface during the collision [32, 33].
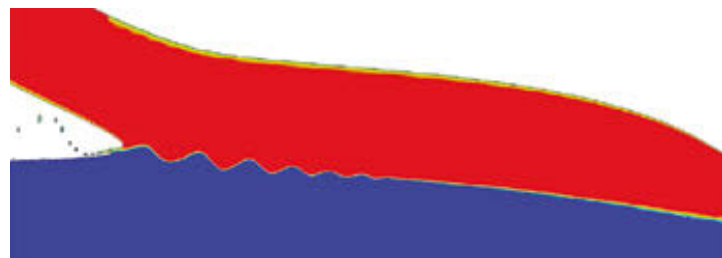

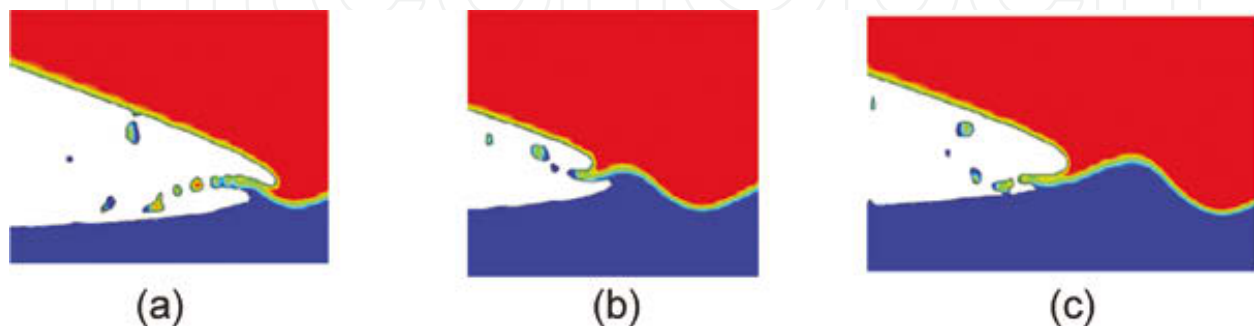**Figure 10.** Eulerian simulation showing the development of wavy pattern at the welded interface.

Figure 11. Eulerian simulation of jetting kinematics during the collision propagation with downward jet in (a) and upward jets in (b) and (c).

5.4. Computation of the thermomechanical phenomena

The plastic work due to the interfacial shearing plays a significant role in the interfacial behaviour. It produces localised heating phenomenon at the vicinity of the excessive sheared zone where a temperature change arises. With the accurate computation of the interfacial deformation, Eulerian simulation captures the interfacial heating while providing accurate predictions in terms of heating location and shape of the heat affected zone (HAZ). **Figure 12** presents a comparison between a computed HAZ and experimental observations. The simulation results exhibit particular HAZ where the highest temperature indicates a potential site of defect's formation. This zone undergoes a thermomechanical softening which is conducive to a development of failure when detrimental conditions (critical strain, stress, damage parameters etc.) occur. Experimentally, along the wavy pattern, formation of voids is observed within the numerically predicted extremely heated sites. Experimental observation of the voids' shapes also concur the shapes of the high temperature distribution during the numerical simulations for the Al/Al joint (**Figure 12a,b**). In the case of Al/Cu combination, Eulerian simulation also reproduces an interfacial heating that corroborates the corresponding experimental observations (**Figure 12c–e**). The computed heating clearly indicates the development of a confined heated layer for Al/Cu joint. The temperature distribution of the layer reveals a convincing shape and size that leads the possibility to predict the formation of intermediate intermetallic phases at the interface. Furthermore, the ejection of significant quantity of material due to the strong interfacial shearing combined with the relatively softer material of the copper than that of aluminium (**Figure 12c–e**) causes a potential detrimental phenomenon that can explain the large experimental cracks (**Figure 12d**). These overall predictions demonstrate the capability of Eulerian simulation to investigate the weldability conditions for MPW by a direct computation of the interfacial behaviour during the collision. Such approach will significantly facilitate the accurate depiction of welding conditions and contribute thereby to the process proficiency.
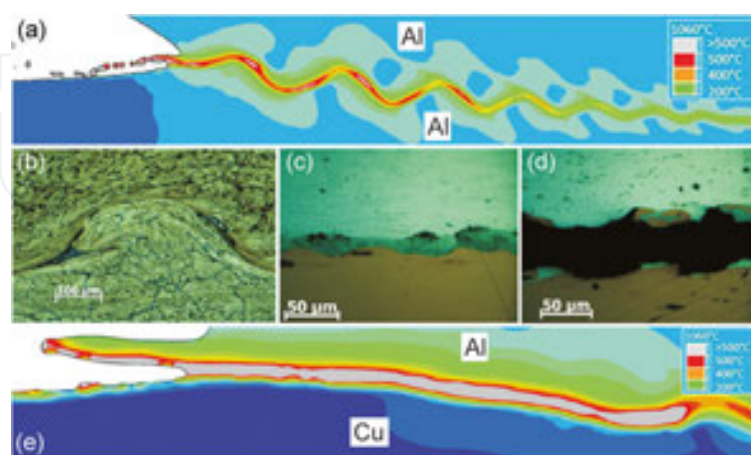

Figure 12. Typical simulation results of the weld natures for (a) similar and (e) dissimilar materials, predicting wavy interface and localised thermal effects. Experimental observations of wave formation in (b) and detrimental phenomena in b–d.

6. Multi-physics computation of the flyer in-flight behaviour

In impact welding, the in-flight behaviour of the flyer determines the collision conditions. Generally, the flyer velocity prior to the impact governs the interfacial phenomena. This is the characteristic parameter that should be known depending on the process and adjustable parameters. Experimental measurements using laser velocimetry methods provide an accurate assessment of the flyer velocity but numerical computation offers a better description of the flyer velocity in terms of spatial and temporal distribution. This section presents a multi-physics computation of the MPW process behaviour. It covers the electromagnetic discharge through the coil and the coupled electromagnetic-mechanical computation of the flyer behaviour. A 3D model is described, including the physical interactions of the process, the governing equations, the resolution procedure, and both boundary and initial conditions. It is employed to show the capability of the model to compute the process behaviour and particularly, the flyer kinematics and macroscopic deformation. Illustrations of spatially distributed impact velocity simulation are presented.

6.1. Governing physics and multi-physics interaction during MPW

Figure 13 describes the multi-physics phenomena involved in the MPW process. The in-flight behaviour of the flyer is mainly governed by the electromagnetic induction and the mechanical response of the material via the Lorentz force while the structural deformation modifies the distribution of magnetic field which in turn affects the electromagnetic interaction between the coil and flyer. This process produces the macroscopic deformation of the structure. Note that the skin depth effect and associated current confinement causes a Joule effect which heats the external part of flyer where the Lorentz force occurs. Generally, the eddy current intensity is high enough, up to several hundred of kA, to generate a strong heating that diffuses within the flyer. A conductive material is expected to involve a good heat transfer and vice versa for a material with low thermal conductivity. Metals such as steel suffer from strong heating due to this phenomenon whereas aluminium or copper seems to limit such heating effect. The consequence of which will make the variance in electromagnetic properties with the temperature that can change the Lorentz force. Therefore, a full physical description of the phenomenon governing the flyer in-flight behaviour should include this electromagnetic-thermal-mechanical interaction. However, under suitable conditions, an electromagnetic-mechanical coupling provides an accurate computation of the flyer kinematics.

The interfacial collision rather involves microscopic phenomenon that can be separately treated using the flyer kinematics given by the electromagnetic-mechanical macroscopic computation. The time-dependent flyer velocity distribution becomes the initial condition for the computation of the impact as previously described in section (Section 5.3). The structural changes involved by both interfacial dynamics and thermal kinetics imply the consideration of specific metallurgical phenomena that decide properties of the joint. However, the multi-physics simulation of the interface can be limited to the mechanical and thermal aspects to reproduce the morphological features of the interface. In the interface simulations (Section 5.3), the mechanical computation describes the interfacial kinematics with the plastic work heating

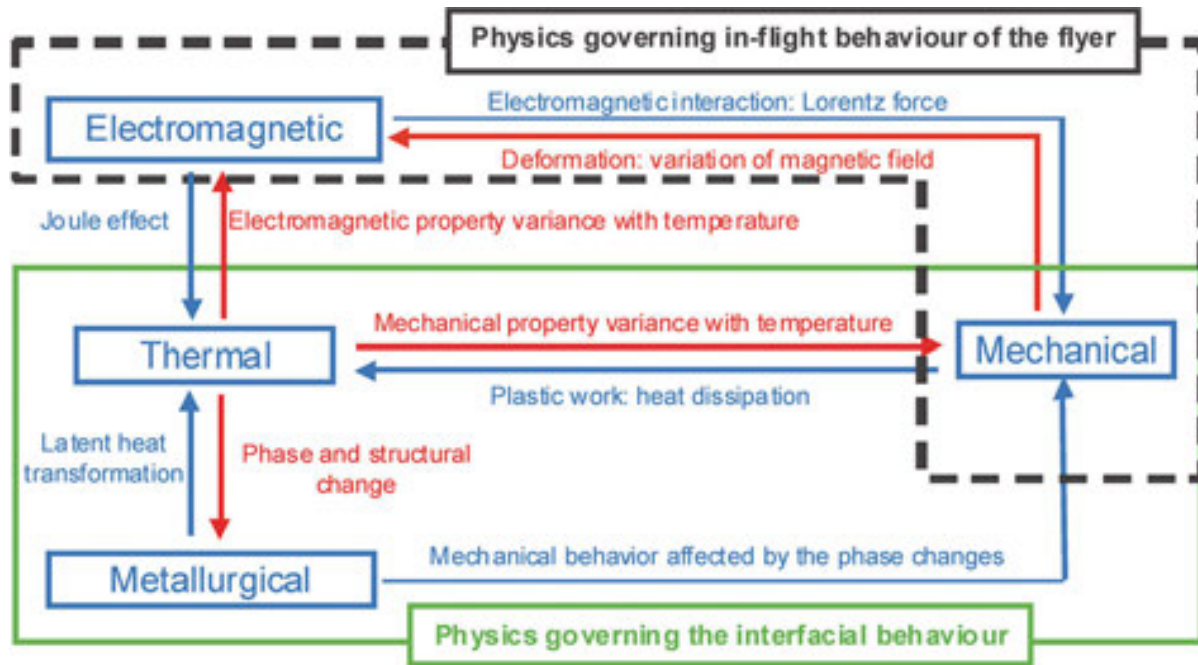while the heat transfer take into account of the mechanical property changes due to the thermal effect.

Figure 13. Synoptic depiction of the multi-physics interactions involved in MPW process.

Moreover, solution time steps are important input parameters that govern the convergence of a simulation. In an electromagnetic-mechanical coupling, that requires for both electromagnetic and mechanical time steps during a simulation. In general the electromagnetic time step $\Delta T \leq p^2/2D$, where p and D are characteristic mesh size and characteristic diffusion time. The characteristic diffusion time D is determined by, $D = 1/\mu\sigma$. The mechanical time step (Δt) is always smaller than the electromagnetic time step, $\Delta t \ll \Delta T$.

6.2. 3D coupled electromagnetic-mechanical model

The electromagnetic problem is governed by the Maxwell equations (Eqs. 10–13) and the electrical and magnetic constitutive relations (Equations 14 and 15). The calculation of magnetic field and eddy current can be performed using these equations.

$$\vec{\nabla} \times \vec{E} = -\frac{\partial \vec{B}}{\partial t}$$

(10)

$$\vec{\nabla} \times \vec{H} = \vec{j} + \varepsilon \frac{\partial \vec{E}}{\partial t}$$

(11)

$$\vec{\nabla} \cdot \vec{B} = 0 \tag{12}$$

$$\vec{\nabla} \cdot \vec{E} = \frac{\rho}{\varepsilon} \tag{13}$$

$$\vec{J} = \sigma \vec{E} + \vec{J}_s \tag{14}$$

$$\vec{B} = \mu \vec{H} \tag{15}$$

In these equations σ, μ and ε respectively represent electrical conductivity, magnetic permeability and electrical permittivity. $\vec{E}$, $\vec{B}$, $\vec{H}$, ϱ, j and $\vec{J}_s$ denote the electric field, magnetic flux density, magnetic field intensity, total charge density, total current density, and source current density respectively. In magnetic pulse forming and welding processes, there involves no charge accumulation and eddy current approximation follow a divergence free current density, those implies $\varrho = 0$ and $\varepsilon \frac{\partial \vec{E}}{\partial t} = 0$.

Due to the divergence condition of Eq. (10) and Eq. (12), they should satisfy the following correlations written in Eq. (16) and Eq. (17) respectively.

$$\vec{E} = -\vec{\nabla}\Phi - \frac{\partial \vec{A}}{\partial t} \tag{16}$$

$$\vec{B} = \vec{\nabla} \times \vec{A} \tag{17}$$

where Φ and $\vec{A}$ are respectively the electric scalar potential the magnetic vector potential. Since the mathematical degree of freedom satisfy the magnetic vector potential $\vec{A}$, a gauge equation is applicable. Using the aforementioned co-relations with the generalized Coulomb gauge condition, $\nabla(\sigma \vec{A}) = 0$, one could separate the vector and scalar potentials as shown in Equation (18) and Equation (19) respectively.

$$\nabla\left(\sigma \vec{\nabla} \Phi\right) = 0 \tag{18}$$

$$\sigma \frac{\partial \vec{A}}{\partial \mu} + \vec{\nabla} \times \left(\frac{1}{\mu} \vec{\nabla} \times \vec{A}\right) + \sigma \vec{\nabla} \Phi = \vec{J}_s \tag{19}$$

Therefore, by solving these Equations 18–19, the two unknowns $\vec{A}$ and Φ in an electromagnetic system can be solved. Finally, based on these solutions procedure and magnetic pressure calculations, Lorentz force is estimated.

In this study, the electromagnetic coupled numerical simulations were carried out using LS-DYNA® package with the solver version R8. The resolution scheme in the electromagnetic-mechanical solver uses both finite element method(FEM) and boundary element method (BEM) [58]. BEM is used toe valuate the surface current and electromagnetic field thus the magnetic field in the air is not required in LS-DYNA® simulations. FEM is used during the computation of eddy current and Lorentz force in the workpieces. At each electromagnetic time step, the electromagnetic and mechanical computations are coupled.

A typical situation of one turn coil with a separate field shaper model is considered as an illustrative 3D simulation case (**Figure 14**). The model consists of solid8 node elements for both workpieces and tools to handle the electromagnetic algorithm in LS-DYNA. The largest element size was selected based on the skin depth and ensured that the element size is sufficient to accurately capture the electromagnetic skin effect (Eq. 3).
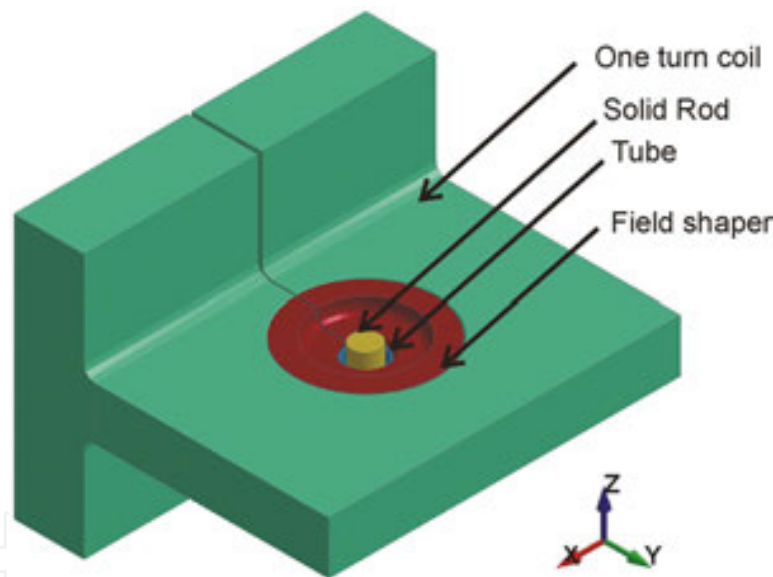

Figure 14. 3D geometrical model.

Material model was described using a simplified Johnson-Cook model (Eq. 20) in the numerical simulations to capture the high strain rate deformation behaviour of the work pieces.

$$\bar{\sigma} = \left(A + B\bar{\varepsilon}^n \right) \left[1 + Cln\left(\frac{\dot{\bar{\varepsilon}}}{\dot{\bar{\varepsilon}}_0} \right) \right] \tag{20}$$

where, $\bar{\sigma}$ and $\bar{\sigma}$ are the von Mises equivalent stress and strain respectively, $\dot{\bar{\varepsilon}}$ is the strain rate. Here $\dot{\bar{\varepsilon}}_0$ is the quasi-static threshold strain rate, treated as equal to *1/s*. *A*, *B*, *C* and *n* are

constants, obtained from literatures, are listed in **Table 1**. Other mechanical, electromagnetic and thermal quantities used in the model are listed in **Table 2**.

Johnson-Cook parameters	A (MPa)	B (MPa)	C	n
Aluminium alloy	352	440	0.0083	0.42
Commercially pure copper	90	292	0.025	0.31

Table 1. Johnson-Cook parameters used to prescribe the constitutive behavior of workpieces.

Material	Part	Density (kg/m^3)	Young's modulus(GPa)	Poisson's ratio	Electrical conductivity (S/m)
Aluminium alloy 2024	Tubeand Rod	2700	73	0.33	1.74×10^7
Commercially pure copper	Rod	8900	124	0.34	3.48×10^7
Copper alloy	Field shaper	7900	210	0.29	2.66×10^7
Steel	Coil	--------------------Rigid-------------------			4.06×10^6

Table 2. Physical properties of the materials and theirs corresponding parts.

6.3. Boundary and initial conditions and other specifications

This section addresses a general procedure for the specification of boundary and initial conditions for an electromagnetic-mechanical model. In the current example, the bottom side of the tube and the top side of the rod are fixed during the simulation. Coil was considered as rigid and fixed during the simulations. The field shaper geometry was placed inside the coil and left free without any boundary conditions to well represent the experimental condition. Automatic surface to surface contact was prescribed between the rod and the tube to capture the contact behaviour during the collision. Electrical conductivity (σ) is defined by electro-magnetic card and the relative magnetic permeability (μ$_r$) was considered as one for all the materials, which indicates that the ferromagnetic effects of materials are neglected during the simulation, whose μ$_r$ values are generally greater than one. The electric and magnetic fields are not only depending on the geometry, assembly configurations and input parameters but also they depend on the input and output surface of the current definitions in a coupled simulation. Therefore, in order to accurately represent the experimental conditions, the exact same connecter point areas are used in the numerical simulations.

In general, an electromagnetic simulation requires to be defined with at least one electrical circuit. In order to define an electrical circuit, a voltage or current curve is applied across the input and output surfaces. Alternatively, the circuit could be specified with R, L, C (resistance, load, and capacitance respectively) parameters of the exterior parts in a circuit without including these parameters of the coil and other components used in a particular simulation.

The specification of the test case and the input current used in the numerical simulations are shown in **Figure 15**.
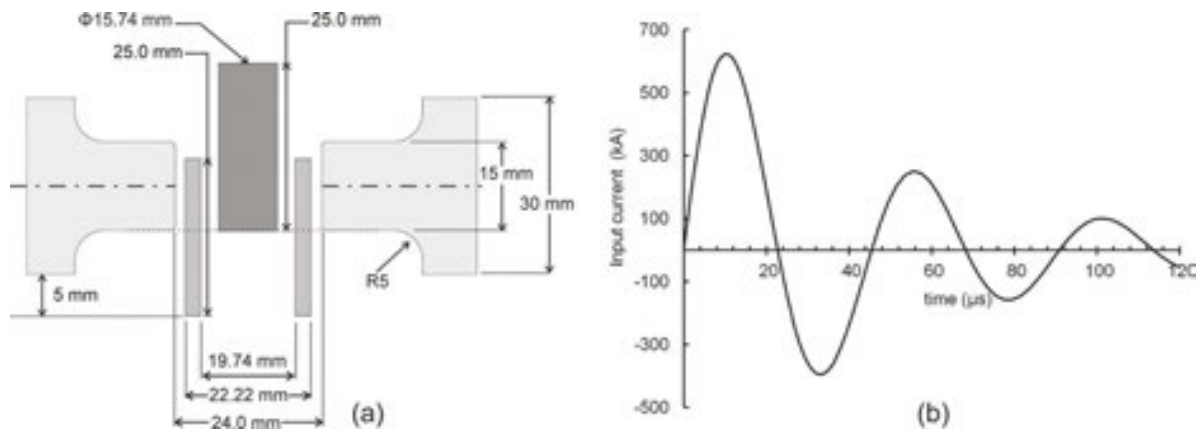

Figure 15. (a) Schematic illustration showing the main working area of the model (field shaper and workpieces) except the coiland (b) the source current used in the model.

6.4. Simulation results of the in-flight behaviour of the flyer

In these numerical simulations, a similar Al/Al and Al/Cu combinations were investigated for their in-flight behaviour in terms of impact velocity and the collision angle at the onset of impact. The properties used in these simulations are corresponding to aluminium alloy 2024 and a commercially pure copper respectively for Al and Cu. The collision angles were calculated estimated on the angle between the radial and longitudinal velocity components (respectively V_r and V_z, see **Figure 17** for detail) from the simulations. The impact velocity was calculated inside of the tube along the longitudinal direction. Sudden change in the resultant velocity was used to determine the onset of the impact and subsequent conditions. That is, immediately at the onset of the impact, the resultant velocity of the tube rapidly reduces. Based on the prediction of the corresponding onset time, resultant velocity and the angle of attack [$tan^1 (Vz/Vr)$] were calculated.

Impact velocity and impact angle against the longitudinal distance from the top edge of the tube are provided in **Figure 16**. The highlighted regions in **Figure 16a** and **b** are able to come in contact during the simulation, which is in agreement with the ~9 mm contact distance observed in experimentally welded samples (**Figure 16c**) obtained under same assembly configuration.

These results suggest that the high speed dynamics for the particular welding case as shown in **Figure 15**. That is, for the particular configuration of the simulation (**Figure 15a**), the top edge of the tube is located slightly above the horizontal mid-plane of the field shaper. This condition causes the highest velocity and the first occurrence of impact slightly below the top edge of the tube. The angle measurements were followed the sign convention given in **Figure 17a**. A closer look of the in-flight collision dynamics shown in **Figure 17b** illustrates the

potential collision condition for the particular assembly configuration used in this numerical study.
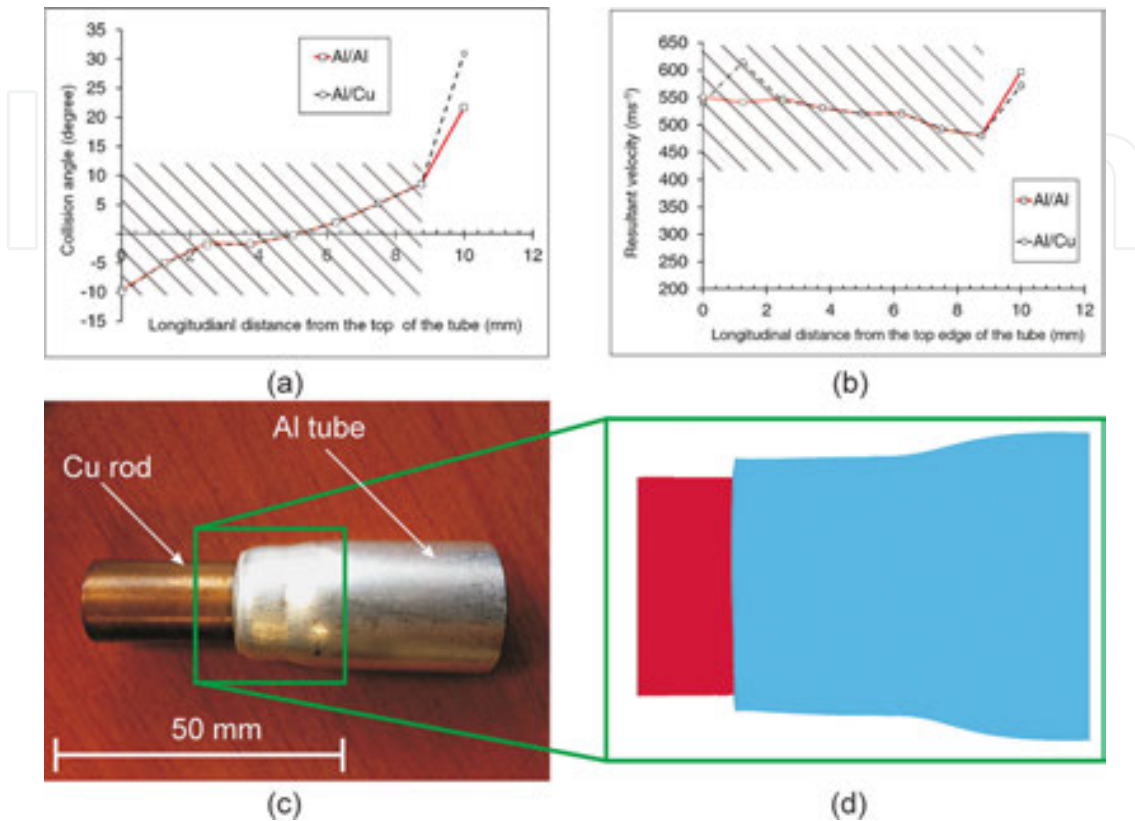

Figure 16. Impact angles along the longitudinal distance from the top edge of the tube for the simulation in (a) and instantaneous resultant velocity at those corresponding points during the onset time in (b). The highlighted regions in (a) and (b) well represent the onset of impact. (c) MPW of Al/Cu sample and (d) final shape of the workpieces from a numerical simulation.
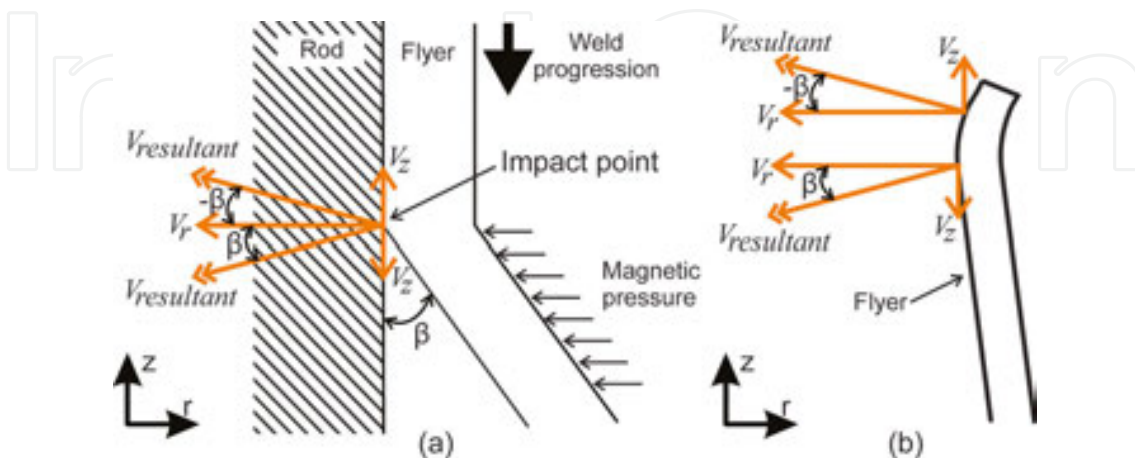

Figure 17. (a) Convention of the angle measurement and (b) a closer look of the in-flight dynamics of the flyer velocity and the impact angle variation.

Although these investigations show that the variance in impact angle and impact velocity, they are not apparent for different inner rods, the influence is suggested as highly depended on the current frequency. That is, one could neglect the difference of the inner rod when predicting the in-flight behaviour at higher current frequencies than that of a critical frequency that can be estimated by equating the first collision time with the full diffusion time of magnetic field through thickness from the exterior to the inner surface of the flyer. In contrast, the difference in the impact condition is not negligible for various inner rods at lower frequencies than that of the critical one. At those lower frequencies, the impact can be influenced by the conductivity of the inner rod [59].
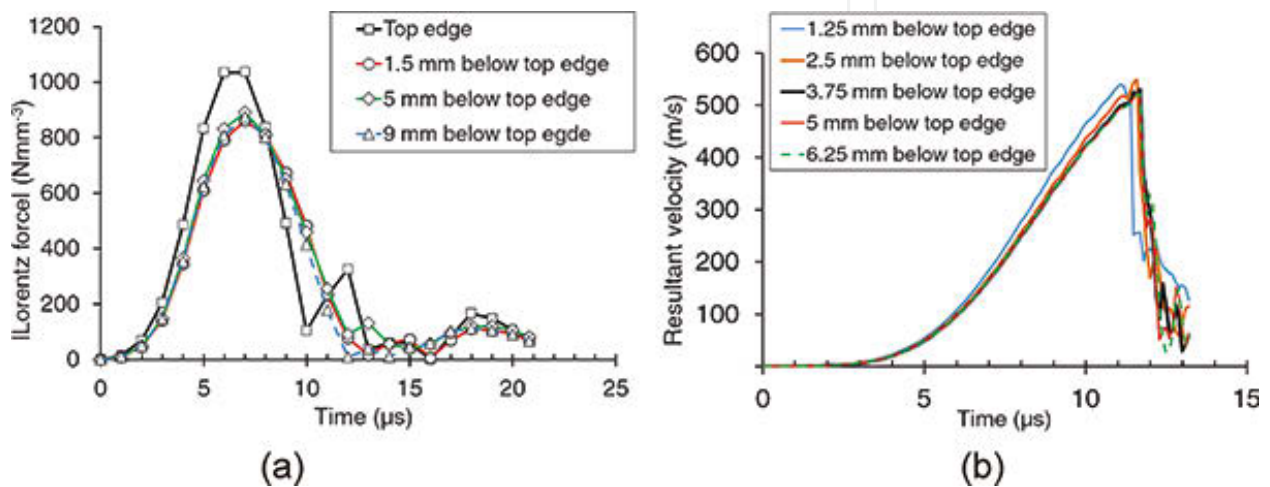

Figure 18. Time dependent radial component of the (a) Lorentz force and (b) velocity obtained from various points on the flyer.

The multi-physics coupled simulations particularly have the benefits of predicting the time dependent the Lorentz body force (**Figure 18a**) and velocity (**Figure 18b**) during the process. Those macroscopic data determines the collision conditions which in turn decides the weld generation. They are crucial for the computation of the interface behaviour during the welding and thus serve as required input condition. Generally, the velocity distribution is appropriate for the interface behaviour simulation that can reproduce physically realistic results (Section 5.4).

7. Conclusions

The magnetic pulse welding is identified as a promising alternative to produce multi material assemblies, while it provides the attractive benefits in terms of cost, reliability, ease of use, flexibility, rate of work, no requirement of consumable and environmental friendliness. The operational conditions were highlighted including the input voltage and initial gap between the flyer and rod were identified as important assembly parameters for a particular overlap configuration of the MPW process. Moreover, the MPW process is also highly influenced by

the current frequency and the electromagnetic skin depth effect. After that interfacial natures and weld variances were investigated for both similar and dissimilar material combinations, where it was identified that the weld variances develop under onset of bonding, wavy interface formation, irregular interfaces, jetting, occurrence of vortices, interfaces with defects and intermetallic formation. The vortex formation is highly apparent in the dissimilar assembly while this also forms the intermetallic phases at the interface as a clear distinct feature from the similar metal assembly. After that, numerical simulations were utilised to capture the interfacial features, this could serve as a potential method to identify the influencing parameters during the weld formation. These simulations well capture the interfacial features including jetting and ejection phenomena. Moreover these simulations reveal the interfacial heating which closely resemble with the defects in terms of side occurrence and shape in those assemblies that indicates these simulations could be utilised to predict the optimum weldability window for various combinations. Finally an investigation of coupled electromagnetic-mechanical simulations provides insight understanding and in-flight kinematics of the flyer that predicts the collision conditions during the MPW process. In summary, all these results indicate the potential outlook and innovative nature of the process among other existing welding technologies. The multi-physics nurture with high speed dynamics and associated high strain deformation particularly makes the process more complex that requires extra attention while manipulating the process. However, promising benefits and the evidence of potentially permanent weld formation always pave the way and keep attracting the manufacturing industries.

Acknowledgements

Author details

T. Sapanathan[1], R. N. Raoelison[2*], N. Buiron[1] and M. Rachik[1]

*Address all correspondence to: rija-nirina.raoelison@utbm.fr

1 Sorbonne universités, Université de Technologie de Compiègne, Compiègne cedex, France

2 Université de Bourgogne Franche Comté, Université de Technologie de Belfort Montbéliard, IRTES EA7274, Belfort, France

References

[1] R. Lapovok, H. P. Ng, D. Tomus, and Y. Estrin, "Bimetallic copper–aluminium tube by severe plastic deformation," *Scripta Materialia*, vol. 66, pp. 1081-1084 2012.

[2] M. Zebardast and A. K. Taheri, "The cold welding of copper to aluminum using equal channel angular extrusion (ECAE) process," *Journal of Materials Processing Technology*, vol. 211, pp. 1034-1043, 2011.

[3] T. Sapanathan, S. Khoddam, S. H. Zahiri, A. Zarei-Hanzaki, and R. Ibrahim, "Hybrid metallic composite materials fabricated by sheathed powder compaction," *Journal of Materials Science*, vol. 51, pp. 3118-3124, 2016.

[4] T. Sapanathan, S. Khoddam, and S. H. Zahiri, "Spiral extrusion of aluminum/copper composite for future manufacturing of hybrid rods: astudy of bond strength and interfacial characteristics," *Journal of Alloys and Compounds*, vol. 571, pp. 85-92, 2013.

[5] M. Knezevic, M. Jahedi, Y. P. Korkolis, and I. J. Beyerlein, "Material-based design of the extrusion of bimetallic tubes," *Computational Materials Science*, vol. 95, pp. 63-73, 2014.

[6] O. Bouaziz, H. S. Kim, and Y. Estrin, "Architecturing of metal-based composites with concurrent nanostructuring: a new paradigm of materials design," *Advanced Engineering Materials*, vol. 15, pp. 336-340, 2013.

[7] D. Embury and O. Bouaziz, "Steel-based composites: driving forces and classifications," *Annual Review of Materials Research*, vol. 40, pp. 213-241, 2010.

[8] T. Sapanathan, S. Khoddam, S. H. Zahiri, and A. Zarei-Hanzaki, "Strength changes and bonded interface investigations in a spiral extruded aluminum/copper composite," *Materials and Design*, vol. 57, pp. 306-314, 2014.

[9] T. Sapanathan, "Fabrication of axi-symmetric hybrid materials using combination of shear and pressure," PhD Thesis (Doctorate), Faculty of Engineering. Department of Mechanical and Aerospace Engineering, Monash University, Melbourne, 2015.

[10] T. Aizawa and M. Kashani, "Magnetic pulse welding (MPW) method for dissimilar sheet metal joints," 57th Annual Assembly of the International Institute of Welding (IIW) 2004, Osaka, Japan.

[11] J. R. Johnson, G. Taber, A. Vivek, Y. Zhang, S. Golowin, K. Banik, *et al.*, "Coupling experiment and simulation in electromagnetic forming using photon doppler velocimetry," *Steel Research International*, vol. 80, pp. 359-365, 2009.

[12] Y. Zhang, S. Babu, and G. Daehn, "Interfacial ultrafine-grained structures on aluminum alloy 6061 joint and copper alloy 110 joint fabricated by magnetic pulse welding," *Journal of Materials Science*, vol. 45, pp. 4645-4651, 2010/09/01 2010.

[13] A. Turner, P. H. Zhang, V. Vohnout, and G. S. Daehn, "Spot impact welding of sheet aluminum," *Materials Science Forum*, vol. 396, pp. 1573-1578, 2002.

[14] T. Aizawa, M. Kashani, and K. Okagawa, "Welding and forming of sheet metals by using magnetic pulse welding (MPW) technique," presented at the 4th International conference on High Speed Forming, Columbus, 2010.

[15] I. K. Middeldorf, "The economic importance of welding and joining in Europe production values, values added and employees," *Düsseldorf, Germany: German Welding Society*, 2009.

[16] K. Middeldorf, "Trends in joining: value added by welding," *Conference Magnetic Pulse Welding and Forming*, Munich, 2008.

[17] V. Lysak and S. Kuzmin, "Lower boundary in metal explosive welding. Evolution of ideas," Journal of Materials Processing Technology, vol. 212, pp. 150-156, 2012.

[18] A. Kapil and A. Sharma, "Magnetic pulse welding: an efficient and environmentally friendly multi-material joining technique," *Journal of Cleaner Production*, vol. 100, pp. 35-58, 2015.

[19] V. Psyk, D. Risch, B. L. Kinsey, A. E. Tekkaya, and M. Kleiner, "Electromagnetic forming—a review," *Journal of Materials Processing Technology*, vol. 211, pp. 787-829, 2011.

[20] P. Pasquale and R. Schäfer, "Robot automated EMPT sheet welding," in *5th International Conference on High Speed Forming*, TU Dortmund, Germany, 2012.

[21] N. Hutchinson, Y. Zhang, G. Daehn, and K. Flores, "Solid state joining of Zr-based bulk metallic glass," *TMS, San Francisco, CA*, 2009.

[22] M. Watanabe, S. Kumai, G. Hagimoto, Q. Zhang, and K. Nakayama, "Interfacial microstructure of aluminum/metallic glass lap joints fabricated by magnetic pulse welding," *Materials Transactions*, vol. 50, pp. 1279-1285, 2009.

[23] M. Kashani, T. Aizawa, K. Okagawa, and Y. Sugiyama, "Welding of manganin and copper sheets by using magnetic pulse welding (MPW) technique," *IEICE Technical Report EMD*, vol. 109, pp. 29-31, 2009.

[24] T. Aizawa, K. Okagawa, and M. Kashani, "Application of magnetic pulse welding technique for flexible printed circuit boards (FPCB) lap joints," *Journal of Materials Processing Technology*, vol. 213, pp. 1095-1102, 2013.

[25] V. Shribman, "Magnetic pulse welding for dissimilar and similar materials," in *3rd International Conference on High Speed Forming*, Dortmund, 2008, pp. 13-22.

[26] V. Shribman, Y. Livshitz, and O. Gafri, "Magnetic pulse welding and joining–a new tool for the automotive," *SAE Technical Paper*, pp. 3401-3408, 2001.

[27] A. K. Jassim, "Magnetic pulse welding technology," in *Energy, Power and Control (EPC-IQ), 2010 1st International Conference on*, 2010, pp. 363-373.

[28] S. Kallee, R. Schäfer, and P. Pasquale, "Automotive applications of electromagnetic pulse technology (EMPT)," *Publication, PSTproducts GmbH*, 2010.

[29] R. Schäfer, P. Pasquale, and S. Kallee, "The electromagnetic pulse technology (EMPT): forming, welding, crimping and cutting," Institute of Welding bulletin, Poland, vol. 58, pp. 50-57, 2014.

[30] Z. Fan, H. Yu, and C. Li, "Plastic deformation behavior of bi-metal tubes during magnetic pulse cladding: FE analysis and experiments," *Journal of Materials Processing Technology*, vol. 229, pp. 230-243, 2016.

[31] W. H. Hayt and J. A. Buck, *Engineering electromagnetics* vol. 7: McGraw-Hill, New York, 2001.

[32] R. Raoelison, N. Buiron, M. Rachik, D. Haye, G. Franz, and M. Habak, "Study of the elaboration of a practical weldability window in magnetic pulse welding," *Journal of Materials Processing Technology*, vol. 213, pp. 1348-1354, 2013.

[33] R. N. Raoelison, T. Sapanathan, N. Buiron, and M. Rachik, "Magnetic pulse welding of Al/Al and Al/Cu metal pairs: consequences of the dissimilar combination on the interfacial behavior during the welding process," *Journal of Manufacturing Processes*, vol. 20, Part 1, pp. 112-127, 2015.

[34] R. Raoelison, N. Buiron, M. Rachik, D. Haye, and G. Franz, "Efficient welding conditions in magnetic pulse welding process," *Journal of Manufacturing Processes*, vol. 14, pp. 372-377, 2012.

[35] R. Raoelison, M. Rachik, N. Buiron, D. Haye, M. Morel, B. Dos Sanstos, *et al.*, "Assessment of gap and charging voltage influence on mechanical behaviour of joints obtained by magnetic pulse welding," in *5th International Conference on High Speed Forming*, Dortmund, 2012, pp. 207-216.

[36] A. Ben-Artzy, A. Stern, N. Frage, and V. Shribman, "Interface phenomena in aluminium–magnesium magnetic pulse welding," *Science and technology of welding and joining*, vol. 13, pp. 402-408, 2008.

[37] R. Raoelison, D. Racine, Z. Zhang, N. Buiron, D. Marceau, and M. Rachik, "Magnetic pulse welding: interface of Al/Cu joint and investigation of intermetallic formation effect on the weld features," *Journal of Manufacturing Processes*, vol. 16, pp. 427-434, 2014.

[38] E. Uhlmann and A. Ziefle, "Modelling pulse magnetic welding processes–an empirical approach," in *4th International Conference on High Speed Forming, Columbus, Ohio, USA*, 2010, pp. 108-116.

[39] A. Nassiri, G. P. Chini, and B. L. Kinsey, "arbitrary lagrangian eulerian fea method to predict wavy pattern and weldability window during magnetic pulsed welding," in *ASME 2015 International Manufacturing Science and Engineering Conference*, Charlotte, North Carolina, USA, 2015.

[40] A. A. Mousavi, S. Burley, and S. Al-Hassani, "Simulation of explosive welding using the Williamsburg equation of state to model low detonation velocity explosives," *International Journal of Impact Engineering*, vol. 31, pp. 719-734, 2005.

[41] S. A. Mousavi and S. Al-Hassani, "Finite element simulation of explosively-driven plate impact with application to explosive welding," *Materials and Design*, vol. 29, pp. 1-19, 2008.

[42] X. Wang, Y. Gu, T. Qiu, Y. Ma, D. Zhang, and H. Liu, "An experimental and numerical study of laser impact spot welding," *Materials and Design*, vol. 65, pp. 1143-1152, 2015.

[43] X. Wang, Y. Zheng, H. Liu, Z. Shen, Y. Hu, W. Li, *et al.*, "Numerical study of the mechanism of explosive/impact welding using smoothed particle hydrodynamics method," *Materials and Design*, vol. 35, pp. 210-219, 2012.

[44] S. A. A. A. Mousavi, "Numerical studies of explosive welding of three-layer cylinder composites-part 2," *Materials Science Forum*, Vol. 580, 2008, pp. 327-330.

[45] A. A. Mousavi, and S. Al-Hassani, "Numerical and experimental studies of the mechanism of the wavy interface formations in explosive/impact welding," *Journal of the Mechanics and Physics of Solids*, vol. 53, pp. 2501-2528, 2005.

[46] A. Nassiri, "Investigation of wavy interfacial morphology in magnetic pulse welding: mathematical modelling, numerical simulation and experimental tests," PhD Thesis (Doctorate), Univseristy of New Hampshire, Durham, NH, 2005.

[47] A. Oberg, J. Schweitz, and H. Olfsson, "Computer modeling of the explosive welding process," in *Proceedings of the 8th International Conference on High Energy Rate Fabrication*, San Antonio, Texas, 1984, pp. 75-84.

[48] A. Nassiri, G. Chini, A. Vivek, G. Daehn, and B. Kinsey, "Arbitrary Lagrangian–Eulerian finite element simulation and experimental investigation of wavy interfacial morphology during high velocity impact welding," *Materials and Design*, vol. 88, pp. 345-358, 2015.

[49] A. Nassiri, G. Chini, and B. Kinsey, "Spatial stability analysis of emergent wavy interfacial patterns in magnetic pulsed welding," *CIRP Annals-Manufacturing Technology*, vol. 63, pp. 245-248, 2014.

[50] S. Kiselev and V. Mali, "Numerical and experimental modeling of jet formation during a high-velocity oblique impact of metal plates," *Combustion, Explosion, and Shock Waves*, vol. 48, pp. 214-225, 2012.

[51] S. Kiselev, "Numerical simulation of wave formation in an oblique impact of plates by the method of molecular dynamics," *Journal of Applied Mechanics and Technical Physics*, vol. 53, pp. 907-917, 2012.

[52] O. Saresoja, A. Kuronen, and K. Nordlund, "Atomistic simulation of the explosion welding process," *Advanced Engineering Materials*, vol. 14, pp. 265-268, 2012.

[53] M. Liu, D. Feng, and Z. Guo, "A modified SPH method for modeling explosion and impact problems," in *APCOM & ISCM*, Singapore, 2013.

[54] S. Kakizaki, M. Watanabe, and S. Kumai, "Simulation and experimental analysis of metal jet emission and weld interface morphology in impact welding," *Materials Transactions*, vol. 52, pp. 1003-1008, 2011.

[55] D. J. Price, "Smoothed particle hydrodynamics: things I wish my mother taught me," in *Advances in Computational Astrophysics: Methods, Tools, and Outcome*, Cefalù, Italy, 2011.

[56] F. Grignon, D. Benson, K. Vecchio, and M. Meyers, "Explosive welding of aluminum to aluminum: analysis, computations and experiments," *International Journal of Impact Engineering*, vol. 30, pp. 1333-1351, 2004.

[57] W. Xu and X. Sun, "Numerical investigation of electromagnetic pulse welded interfaces between dissimilar metals," *Science and Technology of Welding and Joining*, DOI 10.1179/1362171815Y.0000000092, 2015.

[58] I. Çaldichoury and P. L'Eplattenier, EM Theory Manual, Livermore Software Technology Corporation, California, USA, 2012.

[59] T. Sapanathan, K. Yang, R. Raoelison, N. Buiron, D. Jouaffre, and M. Rachik, "Effect of conductivity of the inner rod on the collision conditions during a magnetic pulse welding process, " in 7th International Conference on High Speed Forming, Dortmund, DOI 10.17877/DE290R-16981, 2016.